MULTI-SCALE MODELING OF LOW-DENSITY CARBON-PHENOLIC ABLATORS

N. N. Mansour[1]*, J. Lachaud*[2]*, F. Panerai*[3]*, J. BE. Meurisse*[4]*, J. C. Ferguson*[4]*,*
A. Borner[4]*, J. Monk*[5]*, C. Tang*[1]*, T. Magin*[6]*, M. J. Wright*[1]*, M. Barnhardt*[1]

[1]NASA Ames Research Center (ARC), [2]University of Bordeaux, [3]University of Illinois Urbana-Champaign,
[4]Science & Technology Corp. at ARC, [5]Analytical Mechanics Associates at ARC, [6]von Karman Institute

ABSTRACT

Efforts to build a Predictive Material Modeling framework from the micro-scale to the macro-scale are presented. To accelerate the design cycle process and reduce the need for extensive testing, NASA is developing modeling and simulation tools that enable characterizing material properties and response to hot plasma. At the micro-scale, the Porous Microstructure Analysis (PuMA) framework is developed for up-scaling properties of porous materials from micro-CT (micro-Computed Tomography). In addition, PuMA includes an oxidation module that computes the response of porous materials to the environment. At the macro-scale, a Type 3 material response model implemented in the OpenFOAM framework, Porous-material Analysis Toolbox based on OpenFOAM (PATO) [1], is being developed to model the response of aeroshells during atmospheric entry. To demonstrate the capabilities, results from three-dimensional simulations of a full-scale monolithic- and a tiled-aeroshell of the Mars Science Laboratory (MSL) are presented using trajectory environments from rarefied simulations (using SPARTA), continuum simulations using Data Parallel Line Relaxation (DPLR), and shock radiation using Non-Equilibrium Air (NEQAIR). Results from the simulations using a monolithic- and the tiled-areoshell are compared to the MSL Entry Descent and Landing Instrument (MEDLI) flight data.

Index Terms— MSL, MEDLI, PICA, DSMC, Radiation, Porous materials, Multi-scale, Tomography,

1. INTRODUCTION

Protecting a spacecraft during atmospheric entry is one of the highest risk factors that needs to be mitigated during the design of a space exploration mission. At entry speeds from space, air turns into high-temperature plasma requiring spacecraft Thermal Protection Systems (TPS) to protect the vehicle payload and manage the heat from the freestream flow. For extreme speeds such as return from the Moon or Mars, sacrificial materials such as ablators are the only option as TPS materials. Most modern successful material architectures of spacecraft heatshields use a porous substrate impregnated with phenolic resin. The substrate is designed to be highly porous to minimize weight and heat conduction, but high porosity makes the material susceptible to penetration of hot gases. This is mitigated by filling the large pores of the substrate with small scale porous phenolic to mitigate the rush of hot gases into the protective substrate; in addition, phenolic decomposes when heated, generating gases that block incoming plasma and carry heat away from the spacecraft.

Computational modeling is uniquely critical for designing and certifying TPS given that conditions and loads experienced during an atmospheric entry are often not fully reproducible in ground-based facilities. Computational modeling is necessary in order to extrapolate the available experimental and flight data to planned flight conditions, and to quantify potential failure modes. The full entry systems modeling effort is both multi-physics and multi-scale, and is primarily divided into two categories: aerothermal environment modeling, and material response modeling.

The paper summarizes the various tools used in analysis of the entry stage of a planetary exploration mission. The numerical tools are presented in the context of simulating the MSL mission. Section 2 presents the aerothermal environment modeling tools, including the hypersonic CFD and the estimation of the radiative heating to the vehicle from the shock layer. In Section 3, the approach to developing a material response model is presented, including the micro-scale effort, and the macro-scale material response model. Finally, in Section 4 we present comparison of flight data from the MSL mission to numerical predictions using modeling tools. The outlook for development of high-fidelity modeling is presented in Section 5.

2. AEROTHERMAL ENVIRONMENT

The conventional approach to a mission TPS Verification and Validation (VV) analysis is to focus on peak heating, thus the initial conditions used for material response analysis are provided several seconds after the entry interface (EI) when continuum can be used to estimate the environment. To assess the validity of missing the initial heat pulse stage, the flow environment during the rarefied and the continuum regime stages have been computed. In addition, radiative heat flux from the

shock layer have been used to produce the results presented in Section 4.

The rarefied regime stage of the MSL mission were computed using the Stochastic Parallel Rarefied-gas Time-accurate Analyzer (SPARTA)[2, 3] prior to 48.4 s of entry where the Knudsen number is such that the Navier-Stokes equations can be inaccurate. The DPLR software is used to compute the hypersonic environment for laminar and turbulent boundary layer assumption from 48.4 s up to 100 s after EI along the MSL 08-TPS-02/01a trajectory [4].

2.1. Rarefied-regime Environment

The MSL flight environment was simulated using the following assumptions for the Direct Simulation Monte Carlo (DSMC) simulations: 1) the wall is super-catalytic forcing CO_2 and N_2 recombination to freestream mole fractions, 2) radiative equilibrium wall is assumed with emissivity of 0.89, 3) Mars atmosphere is modeled using 8 species and 24 reactions (12 forward + 12 backward) [5], 4) Park hypersonics correction is applied to the vibrational relaxation, 5) three-temperature model is used, 6) SPARTA uses Variable Soft Sphere (VSS) model with high temperature transport calibration, 6) Parker equation is used for the rotational relaxation, 7) vibrational relaxation uses Millikan-White equation with Park correction, 8) angle of attack varies from 30 degrees at high altitude to 16 degrees after 48 s of entry. We find that the shock standoff distance decreases with decreasing altitude. Strong non-equilibrium in shock is observed at high altitudes. Figure 1 shows the surface and translational temperature from SPARTA at 40 s after EI.

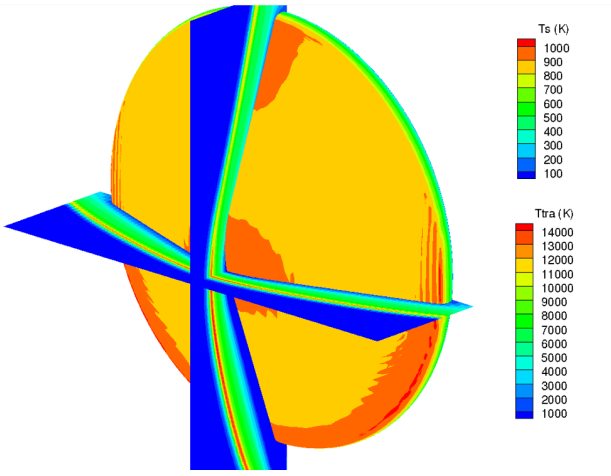

Fig. 1. Surface and translational temperature contours at 40 s of entry computed using DSMC

Material response simulations, described in Section 3, were run to determine if the effect of the rarefied environment was important for the overall entry systems modeling effort. PATO was used to simulate material response of the MSL heatshield in a monolithic and tiled configuration, with the Martian aerothermal environments derived from DPLR only and DSMC+DPLR. For both cases, a uniform initial temperature of 300 K is imposed. Figure 2 shows the surface thermal response at the different MISP locations. The addition of the DSMC results modifies the temperature prediction for the first 60 s after EI. The heating from the DSMC rarefied environment is non-negligible and increases the MISP surface temperature to about 700 K at the first DPLR trajectory point (48.4 s). Figure 3 shows the PATO internal thermal response of the MISP4 thermocouples. Our conclusion is that the in-depth thermal effects in the rarified regime are as important as surface thermal effects especially before 60 s. If interest is focused on peak heating, the initial heating is not critical in determining margins.

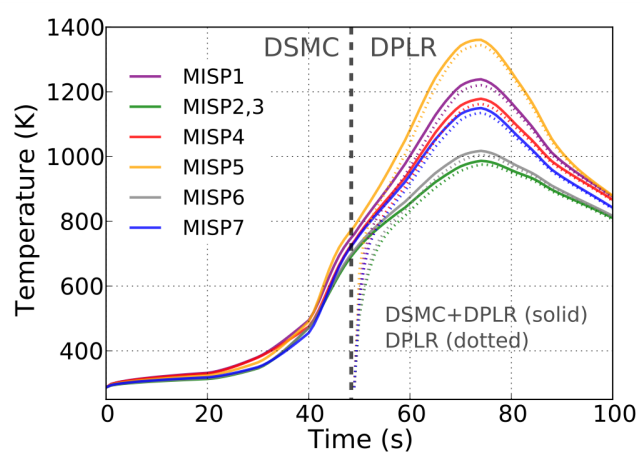

Fig. 2. PATO thermal response at the MISP locations

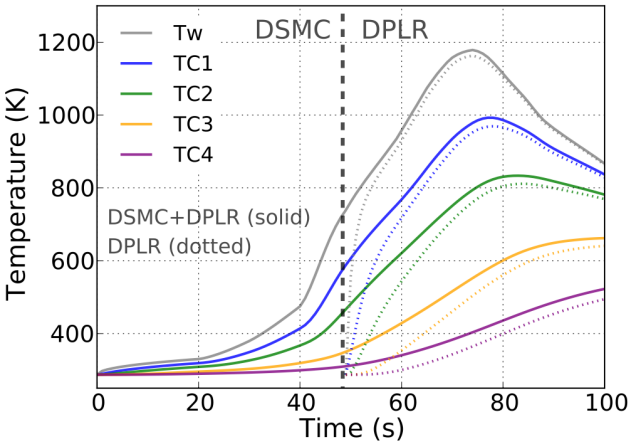

Fig. 3. PATO thermal response at MISP4

2.2. Continuum regime environment

DPLR software is used to compute the hypersonic environment along the MSL entry trajectory for laminar and turbulent boundary layer. The capability of DPLR in accurately predicting the flow field around a Mars entry capsule was demonstrated during past investigations [6]. Surface pressure, heat transfer coefficient and enthalpy at the Boundary Layer Edge (BLE) are extracted from DPLR solutions and are used as inputs to the material response model. We have refined a procedure to project the environmental conditions computed on the hypersonic CFD grid onto the grid used by the material response tool. A linear interpolation scheme in time and a Galerkin projection in space were used to accomplish the projection. The MSL flight environment used in the result section is simulated under the following assumptions: 1) chemical non-equilibrium, 2) thermal non-equilibrium, 3) radiative equilibrium, 5) super-catalytic wall boundary condition, 6) CO_2 and N_2 full recombination, 8 species, 12 reactions, 7) and non-blowing smooth wall.

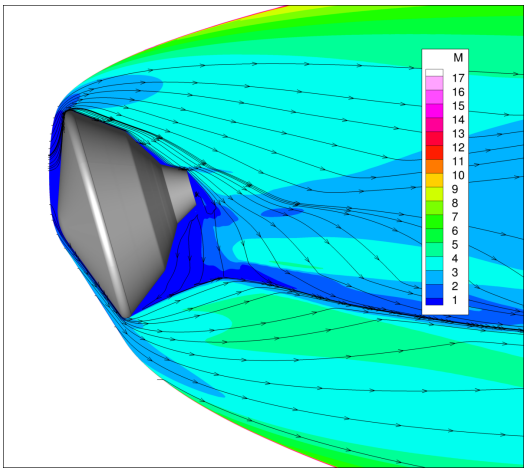

Fig. 4. Mach s for MSL environment at 76.2s[4].

Figure 4 shows the Mach number contour at the pitch plane for the MSL environment computed at 76.2 s after EI [4]. Simulations are performed at 11 discrete times along the MSL 08-TPS-02/01a trajectory: 48.4, 59.1, 64.4, 69.6, 71.5, 73.9, 76.2, 80.5, 84.4, 87.5 and 100.5 s. The numerical results from DPLR are post-processed using the BLAYER code [7] to determine the BLE properties using a curvature-based method. From the BLAYER results, PATO uses the flow conditions to perform the material response. The shear stresses at the surface are omitted as mechanical erosion is not modeled. Figure 5 shows the convective heat flux at the MSL heatshield front surface from the laminar and turbulent environments during peak heating at 76.2 s. In the laminar case, the maximum convective heating is located at the nose and at the windside shoulder. In the turbulent case, the maximum convective heating is located at the leeside outer flank and is

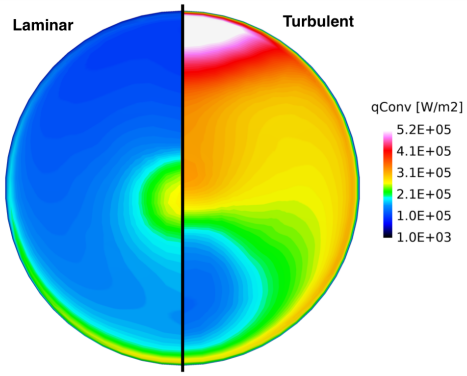

Fig. 5. Convective heat flux for laminar and turbulent environments at 76.2s

.

about 2 times larger than the laminar environment.

2.3. Radiative Environment

The radiative heating is computed on the entire heatshield using NEQAIR) [8] and is added to the full scale material response (see Sec. 3.2) as a surface boundary condition. Again, the AMI method available in OpenFOAM using Galerkin projection is used for the spatial interpolation from the radiation mesh to the material response mesh. The NEQAIR code is one of the original heritage solvers for radiative heating prediction in aerothermal environments.

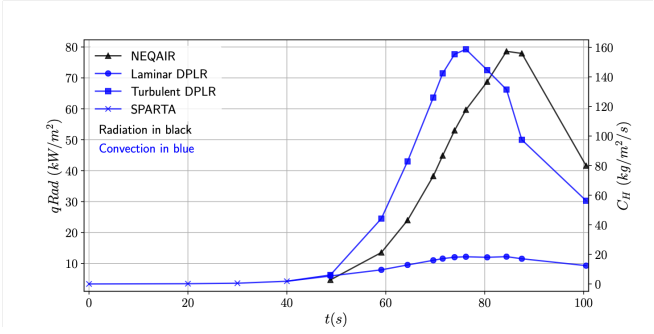

Fig. 6. Radiative and convective inputs over time at MISP2

The radiation analysis is run on all 11 CFD trajectory points at 202 radial points on the half-body heatshield solutions. 172 points used tangential slab method and 30 points used full angular integration methods. Figure 6 shows the evolution in time of the radiative heat flux compared to the convective heat flux. The radiative and convective heat flux have peaks at 78 s and 84 s, respectively. Figure 7 shows the radiative heat flux and the ratio of the radiative heat flux to the total heat flux at the MSL heatshield front surface during the convective peak heating. The maximum radiative heating is located at the leeside shoulder. The total heat flux from Fig.

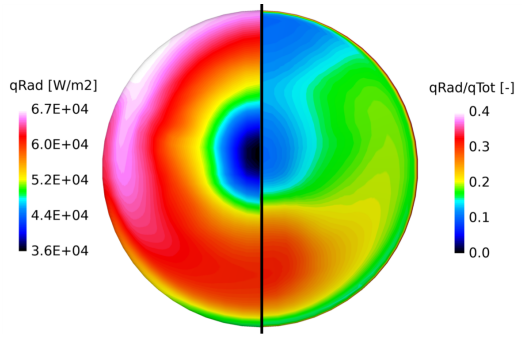

Fig. 7. Radiative heat flux at 75 s[4].

7 is computed using the turbulent aerothermal environment. The radiative heat flux is up to 35% of the total heat flux at 75 s in the windside region showing the importance of adding the radiative environment to the material response simulations.

3. MATERIAL RESPONSE

3.1. Modeling at the micro-scale

High-fidelity full-scale modeling of TPS requires a detailed understanding of the materials properties and behavior under a wide variety of conditions. While many parameters can be derived from carefully designed experiments, others are difficult to measure experimentally. Examples include the evolution of material properties under varying degrees of decomposition, and the properties and response in non-Earth atmospheres. To this end, PuMA [9] has been developed in order to compute the material properties and material response based on microstructural data [10, 11]. The purpose of the software is to be carefully calibrated to available experimental data, and then used to extrapolate beyond the parameter space open to experiments. These properties are then used to inform full-scale material response models, as described in Section 3.2.

Micro-scale modeling requires a detailed representation of a material microstructure. These can be obtained from X-ray micro-CT [12] to provide a high-resolution digital representation of a material micro-structure at sub-micron scale. Voxel datasets (3D images) derived from X-ray tomography provide an excellent computational domain with which to estimate up-scaled material properties [13, 14] to the macro-scale. In PuMA, the computational domains obtained through tomography, or generated computationally, are stored on a Cartesian grid, which is used directly for numerical simulations. This methodology avoids the arduous process of generating volumetric meshes from tomography datasets, which often have extremely complex topologies.

PuMA is a collection of solvers built upon a shared framework of tools and utilities. PuMA can compute basic phenomenological properties such as the porosity, solid volume fractions, specific surface area, and mean intercept length (an estimation of mean pore diameter). It can also provide various upscaled transport properties. For example, a critical property for modeling TPS response at the full-scale is the effective thermal conductivity of the composite materials. PuMA includes two solvers to compute the solid (and electrical) conductivity: the Explicit Jump method of Wiegmann et. al. [15] and a Finite Volume formulation [9]. Both numerical methods impose a temperature gradient across the material and compute the steady-state temperature profile. From this, the steady-state heat flux and the effective thermal conductivity can be determined.

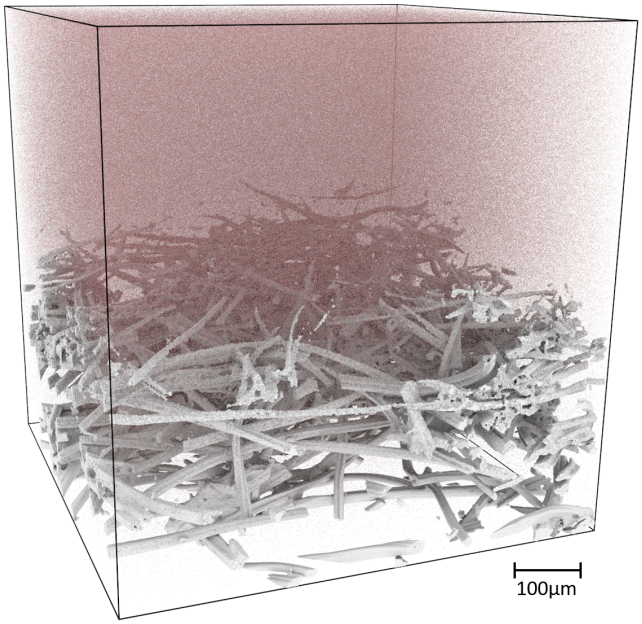

Fig. 8. Mixed-regime micro-scale oxidation simulation, showing a reaction depth of approximately 300 μm

Another important capability of PuMA is modeling material response at the micro-scale. A micro-scale oxidation model [16, 17] is available [18], for simulation of decomposition at the micro-scale. Diffusion is simulated via a particle method, with particle-particle collisions estimated in the same fashion as for the tortuosity solver. The material is stored on a Cartesian grid, and particle-surface collisions with the immersed boundary are determined via a linear interpolation method. Reaction events are determined via a sticking probability law, and the weights on the Cartesian grid are modified accordingly. This methodology captures material recession an fiber thinning. The method has been used to estimate the oxidation depth at a variety of entry conditions [18], and to study the effects of carbonized phenolic resin on the decomposition behavior [19]. An example of an oxidation simulation is shown in Fig. 8, in which FiberForm, the carbon fiber substrate of PICA, is oxidized in the mixed-regime.

3.2. Modeling at the macro-scale

The full-scale material response computational model is a generic heat and mass transfer model for porous reactive materials containing several solid phases and a single gas phase [20]. The detailed chemical interactions occurring between the solid phases and the gas phase are modeled at the pore scale assuming Local Thermal Equilibrium (LTE): solid pyrolysis, pyrolysis species injection in the gas phase, heterogeneous reactions between the solid phases and the gas phase, and homogeneous reactions in the gas phase. The chemistry models are integrated in a macroscopic model derived by volume-averaging the governing equations for the conservation of solid mass, gas mass, species (finite-rate chemistry) or elements (equilibrium chemistry), momentum, and energy. This generic model is implemented in PATO [1], a C++ top level module of the open source computational fluid dynamics software program OpenFOAM. The open source third party library Mutation++, produced by the von Karman Institute for Fluid Dynamics, is dynamically linked to compute equilibrium chemistry compositions and thermodynamic and transport properties [21]. Gas surface interactions are modeled using equilibrium chemistry models that are preferred for design due to the lack of reliability of available finite-rate chemistry models and data. The equilibrium chemistry model of PATO has been shown to perfectly reproduce one-dimensional design tool results [22]. PATO has been carefully verified against the Fully Implicit Ablation and Thermal Analysis (FIAT) software, NASA's state-of-the-art-code for TPS response modeling, extensively validated through arcjet tests and flight data [23].

3.2.1. Full-scale modeling

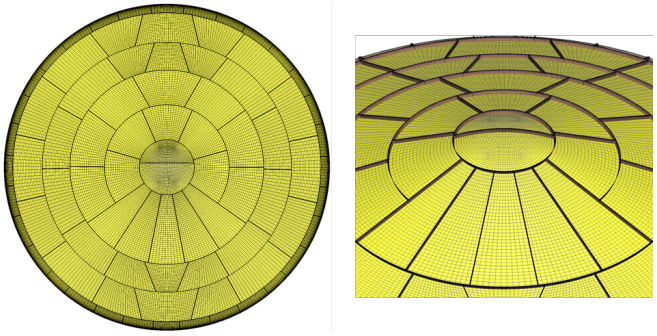

Fig. 9. MSL tiled heatshield mesh with PICA in yellow and RTV in brown

The MSL aeroshell is a 4.5 m diameter, 70 degree half-angle sphere-cone forebody, with triconic afterbody. The distribution of the 113 tiles composing the forebody heatshield is presented in Fig. 3. The TPS was assembled using a stacking of materials as detailed in [24]. A uniform PICA layer of 31.75 mm thickness was used along the entire heatshield. The heatshield surface geometry used in PATO was extracted from the computational domain used in DPLR. The PATO computational mesh has approximately 2M cells. The minimum cell size is 1 mm. The mesh (shown in Fig. 9) is separated into 2 material regions: porous tiles (yellow) and gap filler between the tiles (orange). The porous tiles are made of PICA, while the gap filler is made of RTV. In building the computational model for this study, we made the following simplifying assumptions, which will be addressed in follow-up studies. The surface coating applied onto the PICA heatshield and its effects on the material response are neglected. The gap filler, here meshed with two cells of 1 mm each, is assumed to be a non-charring and non-receding phase. Therefore, as opposed to the real case, where the charring process of the gap filler would yield a porous carbonaceous structure, here the interface is impermeable to gases and only conductive heat transfer is allowed through it. The non-receding simplification, also to be refined in future investigations, was inspired by the minimal observed recession during arc-jet testing of the gap filler [24].

3.2.2. Spatial Interpolation

A spatial interpolation procedure is developed to interface the PATO and DPLR grids. While DPLR uses a structured mesh for the computation of the aerothermal environment, PATO adopts an unstructured moving mesh technique for the material response. PATO's moving grid system allows for shape changes due to surface recession. A spatial interpolation between the DPLR and PATO grids is performed at discrete time steps for the different meshes. AMI of OpenFOAM was used for such purpose; AMI enables interfacing adjacent, disconnected mesh domains using Galerkin projection [25].

Figure 10 shows an illustration of the spatial interpolation for two different regions of the heatshield forebody surface at 90 s of the MSL trajectory. The thick black lines represent the gap filler between two adjacent PICA tiles. The environment grid is presented in pink color, while the material grid is shown in black. It is noticed that, at the outer flank region (left image of Fig. 10), the cell size of the two grids is similar. In contrast, the right image of Fig. 10 shows large differences between mesh resolutions at the nose region. This difference causes small numerical fluctuations at the nose region, which are deemed negligible for the present study. Future improvement shall include the capability to adapt the hypersonic CFD grid to better match the porous material response mesh. Figure 10 also shows the surface shape change due to material ablation. The differential recession between the non-receding gap filler and the ablative porous material promotes the formation of a fence. This result closely resembles the fencing phenomenon observed experimentally when testing PICA samples with RTV-bonding interfaces **??**. The fencing phenomenon poses design challenges as it is a potential promoter of transition to turbulence [26]. If a detailed material

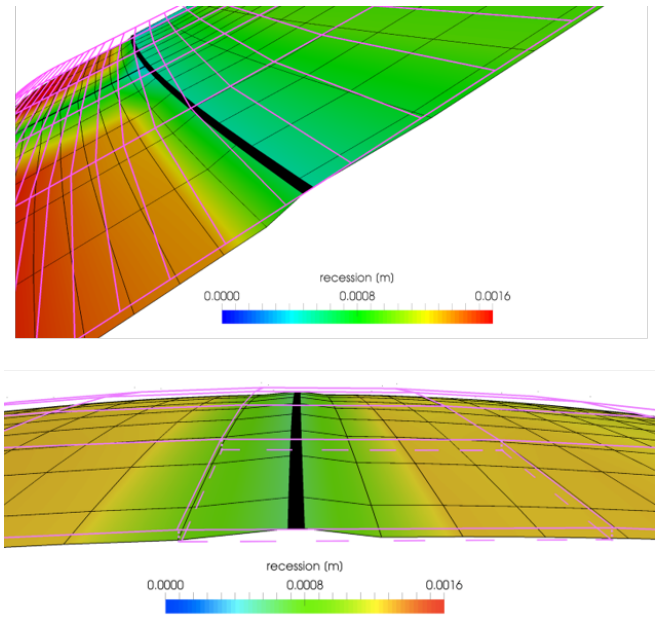

Fig. 10. Spatial interpolation between the environment grid (pink) and the material grid (black) at 90 s

model for the gap filler were added to the CFD simulation, the current technology would improve prediction models of the fencing phenomenon along a varying heat flux trajectory. The present simulation technology constitutes a first step towards the prediction of the tile interface fencing phenomenon, which is a potential promoter of transition to turbulence at hypersonic conditions. Realistic finite-rate chemistry models for both PICA and RTV will be fundamental for such predictive effort. Fences can also enhance surface heating for laminar and turbulent flows.

3.2.3. Surface Temperature and Recession

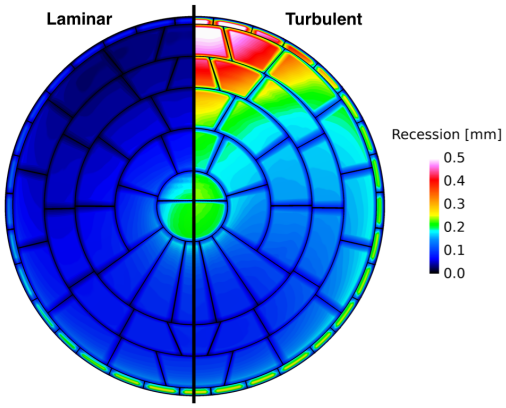

Fig. 11. 3D view of surface recession for MSL entry at 70 s

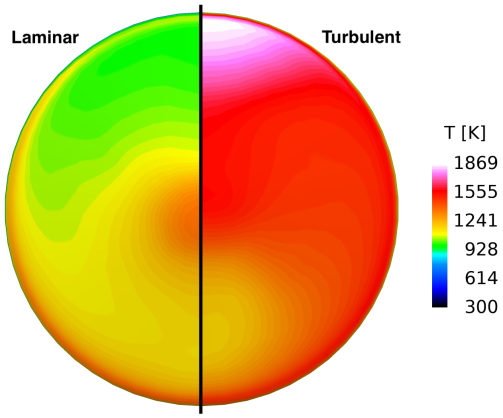

Fig. 12. 3D view of surface temperature for MSL entry at 70 s

Figure 11 shows the MSL front surface recession at 70 s after EI for laminar and turbulent environments. These recession results are in line with MSL observations. During the MSL mission, all the MEDLI Integrated Sensor Plugs (MISP) thermocouples survived the Mars entry. The thermocouple closest to the heatshield surface at the different MISP locations were measured by X-Ray imaging at about 2.53 mm, which indicates that the maximum recession at those locations were less than 2.53 mm. The laminar case gives a higher recession at the nose and at the windside shoulder. The turbulent case shows higher recession at the leeside outer flank. Interestingly, there is an increasing differential recession between the porous material and the tile interface. Figure 12 shows the MSL front surface temperature at 70 s after EI for laminar and turbulent environments. Higher temperature regions are observed at the windside outer flank and nose for the laminar environment and at the leeside outer flank for the turbulent environment.

3.2.4. Internal Velocity

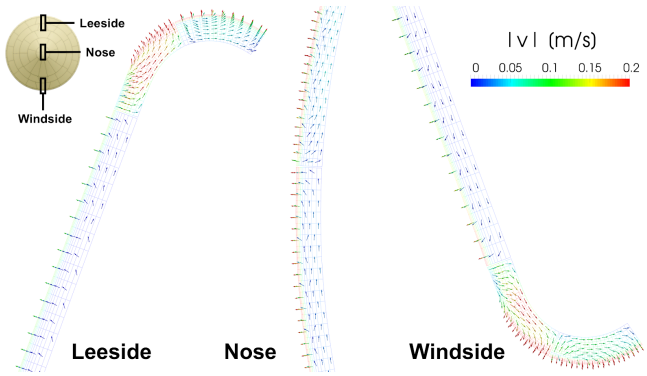

Fig. 13. Velocity field at cross-sections of different heatshield regions (85s)

Figure 13 shows the velocity field inside the heatshield at the leeside, nose and windside regions at 85 s when the maximum stagnation pressure occurs during MSL entry. The in-depth velocity within the porous tiles is chiefly driven by the pressure differences within the tiles, as postulated by Darcy's formulation of the momentum equation. For the three locations, shown in Fig. 13, we observe an outward velocity normal to the surface, due to the outflow of pyrolysis gases. Across the entire heatshield thickness, the transverse velocity is less than 1 mm/s at the leeside flank, at the nose and at the windside flank regions. Such a low transverse velocity suggests that the use of a 1D model is an accurate approximation of the 3D isotropic material behavior in these regions. Conversely, the velocity at the leeside and windside outer flank regions, where the geometry presents strong curvatures, reaches 0.2 m/s in the transverse direction. In these regions, a 1D model would be unsuitable to correctly predict the flow transport.

3.2.5. In-depth Temperature

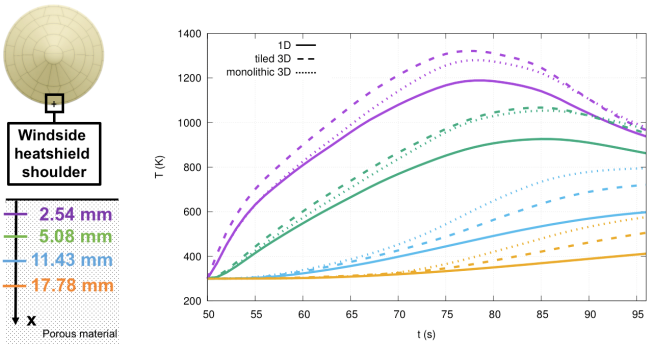

Fig. 14. Comparison of the temperature for different heatshield configurations at the windside shoulder region

Figure 14 shows in-depth temperature history at the windside outer flank. The temperature is plotted at four in-depth positions, for three cases with isotropic material properties: 1D material response, 3D material response with tiles and 3D monolithic material response. The same through-thickness grid resolution is used in the 1D and 3D simulations. A grid convergence study, performed at the probe locations, showed that the relative difference between the in-depth resolution of 10 and 100 cells is less than 3%. For the windside outer flank (Fig. 14), where 3D flow effects are pronounced, the 1D case underpredicts the temperature beneath the surface by a maximum of 18% compared to the tiled configuration and a maximum of 28% compared to the monolithic configuration. It is expected that, using transverse anisotropic material properties (e.g. anisotropic effective thermal conductivity and permeability) instead of the isotropic material assumption adopted in the present case, the observed differences would be amplified. Our simulations show that, for the MSL heatshield geometry, 3D in-depth flow velocity effects are more pronounced at the outer flank region. At the nose and flank regions, where the MISP sensors are located, the in-depth flow transport is basically one-dimensional since 1D and 3D material response simulations yielded very close results for the in-depth material temperature. This result confirmed the suitability of a 1D model for heatshield sizing purposes and for MISP analysis in those regions.

4. COMPARISON TO FLIGHT DATA

The MEDLI suite on MSL offers unique in-flight validation data for models of atmospheric entry and material response. MEDLI recorded, among others, time-resolved in-depth temperature data of PICA using thermocouple sensors assembled in the MISP. These measurements have been widely used in the literature as a validation benchmark for state-of-the-art ablation codes [24, 27]. Each MISP carried thermocouple sensors (labelled as TC), which are used as reference points in the present study. MISP4 is located near the stagnation point on the windside of the heatshield, while MISP2 is located on the leeside of the heatshield. The following 1D PATO material response results use elemental conservation and equilibrium chemistry. Figure 14 shows the PATO thermal response at MISP2. The MISP2 TC data is located between the PATO results from laminar and turbulent environments. The comparison of the flight data and the PATO results indicates that the aerothermal environment seems to be in a transitional regime at MISP2. Figure 15 shows the PATO thermal response at MISP4. The MISP4 TC1 data is higher at the heating peak than the PATO results, showing that the aerothermal environment underpredicts the peak heating near the stagnation point.

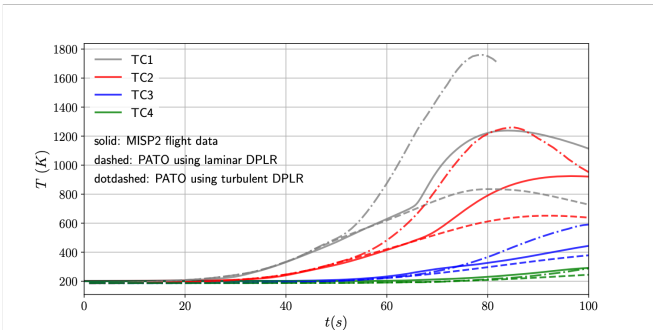

Fig. 15. Comparison between flight data and PATO simulations at MISP2

Clearly, the current models for Mars entry need improvements. Extensive efforts to identify sources of discrepancies are being supported under the Entry System Modeling (ESM) project[28]. These include efforts to identify the effects of NuSil on the material response. The MSL aeroshell, as flown, was sprayed with NuSil, a silicone coating used to reduce par-

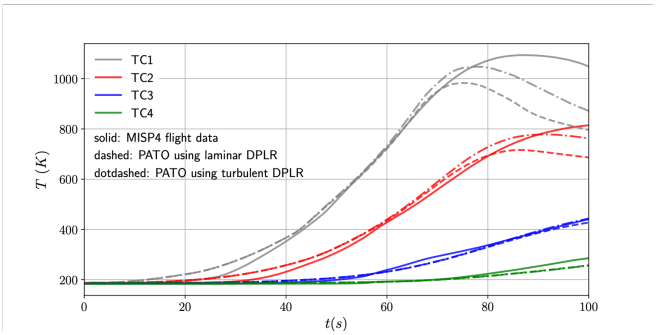

Fig. 16. Comparison between flight data and PATO simulations at MISP4

ticulate shedding. While the spraying did not degrade the performance of the TPS, it has changed gas/surface interactions and there the in-depth response of the material.

5. CONCLUSION AND OUTLOOK

Good progress has been made towards multi-physics, high-fidelity modeling of a spacecraft aeroshell during atmospheric entry that enables refinement of margin policies imposed on final designs. However, many challenges remain for a complete mastery of this multi-physics challenge. With advancement in computational capabilities, interest at NASA has emerged in tackling the ground to flight extrapolation major challenge experienced during mission designs. We find that computational technology is outpacing our fundamental understanding and models to mitigate known challenges. Areas that need immediate focus are investments in modeling spallation, intumescence, strong multi-physics coupling, Micro Meteorite-Orbital Debris (MMOD) impact effects, etc. Design of entry systems is at the cusp of a major shift similar to one experienced in aeronautics during the late 1970's. In the next decade we will find that TPS designs will rely more and more on simulations than ground testing.

6. REFERENCES

[1] J. Lachaud and N. N. Mansour, "Porous material analysis toolbox based on openfoam and applications," *Journal of Thermophysics and Heat Transfer*, vol. 28, no. 2, pp. 191–202, 2014.

[2] SJ Plimpton, SG Moore, A Borner, AK Stagg, TP Koehler, JR Torczynski, and MA Gallis, "Direct simulation monte carlo on petaflop supercomputers and beyond," *Physics of Fluids*, vol. 31, no. 8, pp. 086101, 2019.

[3] Michael A Gallis, John R Torczynski, Steven J Plimpton, Daniel J Rader, and Timothy Koehler, "Direct simulation monte carlo: The quest for speed," in *AIP Conference Proceedings*. AIP, 2014, vol. 1628, pp. 27–36.

[4] Jeremie BE Meurisse, Jean Lachaud, Francesco Panerai, Chun Tang, and Nagi N Mansour, "Multidimensional material response simulations of a full-scale tiled ablative heatshield," *Aerospace Science and Technology*, vol. 76, pp. 497–511, 2018.

[5] Robert Alan Mitcheltree and Peter A Gnoffo, "Wake flow about the mars pathfinder entry vehicle," *Journal of Spacecraft and Rockets*, vol. 32, no. 5, pp. 771–776, 1995.

[6] Karl Edquist, Artem Dyakonov, Michael Wright, and Chun Tang, "Aerothermodynamic environments definition for the mars science laboratory entry capsule," in *45th AIAA Aerospace Sciences Meeting and Exhibit*, 2007, p. 1206.

[7] David A Saunders and Dinesh K Prabhu, "Blayer user guide," 2018.

[8] Chul Park, "Nonequilibrium air radiation (nequair) program: User's manual," *NASA Technical Memorandum*, 1985.

[9] Joseph C Ferguson, Francesco Panerai, Arnaud Borner, and Nagi N Mansour, "Puma: the porous microstructure analysis software," *SoftwareX*, vol. 7, pp. 81–87, 2018.

[10] Nagi N Mansour, Francesco Panerai, Alexandre Martin, Dilworth Y Parkinson, Alastair A MacDowell, Tony Fast, Gerard Vignoles, and Jean Lachaud, "A new approach to light-weight ablators analysis: from micro-tomography measurements to statistical analysis and modeling," in *Proc. 44th AIAA Thermophysics Conference, American Institute of Aeronautics and Astronautics, AIAA-2013-2768*, 2013.

[11] Francesco Panerai, Joseph C Ferguson, Jean Lachaud, Alexandre Martin, Matthew J Gasch, and Nagi N Mansour, "Micro-tomography based analysis of thermal

conductivity, diffusivity and oxidation behavior of rigid and flexible fibrous insulators," *International Journal of Heat and Mass Transfer*, vol. 108, pp. 801–811, 2017.

[12] Jiang Hsieh, *Computed tomography: principles, design, artifacts, and recent advances*, vol. 114, SPIE press, 2003.

[13] Eric Maire, "X-ray tomography applied to the characterization of highly porous materials," *Annual Review of Materials Research*, vol. 42, pp. 163–178, 2012.

[14] Christoph H Arns, Mark A Knackstedt, M Val Pinczewski, and WB Lindquist, "Accurate estimation of transport properties from microtomographic images," *Geophysical research letters*, vol. 28, no. 17, pp. 3361–3364, 2001.

[15] A Wiegmann and A Zemitis, "EJ-HEAT: A fast explicit jump harmonic averaging solver for the effective heat conductivity of composite materials," *Fraunhofer-Institut für Techno-und Wirtschaftsmathematik, Fraunhofer (ITWM)*, 2006.

[16] Jean Lachaud, Yvan Aspa, and Gérard L Vignoles, "Analytical modeling of the steady state ablation of a 3d c/c composite," *International Journal of Heat and Mass Transfer*, vol. 51, no. 9-10, pp. 2614–2627, 2008.

[17] J. Lachaud and G.L. Vignoles, "A brownian motion technique to simulate gasification and its application to C/C composite ablation," *Computational Materials Science*, vol. 44, no. 6, pp. 1034–1041, 2009.

[18] Joseph C Ferguson, Francesco Panerai, Jean Lachaud, Alexandre Martin, Sean CC Bailey, and Nagi N Mansour, "Modeling the oxidation of low-density carbon fiber material based on micro-tomography," *Carbon*, vol. 96, pp. 57–65, 2016.

[19] Joseph C. Ferguson, Francesco Panerai, Jean Lachaud, and Nagi N. Mansour, "Theoretical study on the micro-scale oxidation of resin-infused carbon ablators," *Carbon*, vol. 121, pp. 552 – 562, 2017.

[20] J Lachaud, JB Scoggins, TE Magin, MG Meyer, and NN Mansour, "A generic local thermal equilibrium model for porous reactive materials submitted to high temperatures," *International Journal of Heat and Mass Transfer*, vol. 108, pp. 1406–1417, 2017.

[21] James B Scoggins and Thierry E Magin, "Development of mutation++: Multicomponent thermodynamic and transport properties for ionized plasmas written in c++," in *11th AIAA/ASME joint thermophysics and heat transfer conference*, 2014, p. 2966.

[22] Jean Lachaud, Tom van Eekelen, James B Scoggins, Thierry E Magin, and Nagi N Mansour, "Detailed chemical equilibrium model for porous ablative materials," *International Journal of Heat and Mass Transfer*, vol. 90, pp. 1034–1045, 2015.

[23] Ali D Omidy, Francesco Panerai, Alexandre Martin, Jean R Lachaud, Ioana Cozmuta, and Nagi N Mansour, "Code-to-code comparison, and material response modeling of stardust and msl using pato and fiat," *NASA Technical Memorandum*, 2015.

[24] Todd R White, Milad Mahzari, Deepak Bose, and Jose A Santos, "Post-flight analysis of mars science laboratorys entry aerothermal environment and thermal protection system response," in *44th AIAA Thermophysics Conference*, 2013, p. 2779.

[25] PE Farrell and JR Maddison, "Conservative interpolation between volume meshes by local galerkin projection," *Computer Methods in Applied Mechanics and Engineering*, vol. 200, no. 1-4, pp. 89–100, 2011.

[26] Karl T Edquist and Brian R Hollis, "Mars science laboratory heatshield aerothermodynamics: design and reconstruction," in *44th AIAA Thermophysics Conference*, 2013, p. 2781.

[27] Milad Mahzari, Robert D Braun, Todd R White, and Deepak Bose, "Inverse estimation of the mars science laboratory entry aeroheating and heatshield response," *Journal of Spacecraft and Rockets*, vol. 52, no. 4, pp. 1203–1216, 2015.

[28] Michael Wright, Monica F Hughes, Michael Barnhardt, and Anthony M Calomino, "An overview of technology investments in the nasa entry systems modeling project," in *53rd AIAA Aerospace Sciences Meeting*, 2015, p. 1892.